Isothermal Oxidation Behavior of Novel Al$_2$O$_3$ / NiCrAlY / Ti$_3$Al System at 850°C

ALEXANDRA BANU[1], ALEXANDRU PARASCHIV[2], SIMONA PETRESCU[3], IRINA ATKINSON[3], ELENA MARIA ANGHEL[3*], MARIA MARCU[3*]

[1]Politehnica University of Bucharest, Faculty of Industrial and Robotic Engineering, 313 Splaiul Independentei, 060032, Bucharest, Romania
[2]COMOTI – Romanian Research Development Institute for Gas Turbines, 220 Iuliu Maniu, 061126, Bucharest, Romania
[3]Institute of Physical Chemistry "Ilie Murgulescu", Departament of Electrochemistry and Corrosion, 202 Splaiul Independentei, 060021, Bucharest, Romania

Abstract: The novel Al$_2$O$_3$ / NiCrAlY /α_2-Ti$_3$Al system obtained by APS technique was tested against long (500h) isothermal oxidation at 850°C in air for prospective use in aerospace applications. EDX-SEM, X-ray diffraction (XRD) and Raman investigations were conducted to substantiate structural, textural and mass gain modifications underwent by the Al$_2$O$_3$ / NiCrAlY /α_2-Ti$_3$Al system in comparison with bare α_2-Ti$_3$Al and NiCrAlY /α_2-Ti$_3$Al system. Improved oxidation resistance of the double-coated system is based on moderate oxygen and thermal barrier role played by the mixture of δ - and α-Al$_2$O$_3$ present in the top ceramic coat.

Keywords: isothermal oxidation, titanium aluminide, diffusion barrier

1. Introduction

High-temperature structural materials for aerospace and automotive purposes [1] operate in one of the harshest environments being exposed to severe mechanical loads, high temperature, as well as corrosion and erosion conditions. That enforces continuous development of new generations of TiAl alloys with improved properties (low density, high specific strength and melting temperature, good creep resistance, excellent fireproof performance) in comparison with Ti-alloys which replaced Ni-superalloys [2,3]. Both conventional Ti-alloys and titanium aluminide alloys, especially in alpha form with rich titanium content α_2-Ti$_3$Al, show poor oxidation and corrosion resistance at elevated temperatures in air as well as in marine environments at ambient temperature [1-6]. Choice of titanium richer alloys, TiAl (γ phase), Ti$_2$AlNb (*o-ortho* phase) and α_2-Ti$_3$Al alloys, is ruled by their superior mechanical characteristics [7, 8]. At the time when extensively studied Ti-48Al-2Nb-2Cr alloy was used for the first time in 2006 as rotating parts of a Boeing engine [3], application of the α_2-Ti$_3$Al alloys with unsatisfactory oxidation resistance at service temperature of 800-1000°C has been limited [3,8]. The latter alloys form a mixed unprotective layer of TiO$_2$ and Al$_2$O$_3$ during exposure at high temperature in air and/ or oxygen in contrast with dense protective alumina scales, formed onto the richer aluminum alloys, which act as an effective diffusion barrier against further oxidation of the titanium aluminide support [1]. Despite the fact that Al$_2$O$_3$ is more stable than TiO$_2$, faster rate of the TiO$_2$ formation was recorded at beginning of the oxidation process of titanium aluminides [9].

Addition of other elements (Nb, Mo, Cr, Y, etc.), surface treatment and /or coating deposition on the surface of a α_2-Ti$_3$Al base alloy were developed in order to increase its oxidation resistance and prevent overheating of the base material [3]. Commonly, high-temperature doped-titanium alloys rely, for their resistance against oxidation attack, on formation of oxide scales with highly protective properties, i.e., Al$_2$O$_3$, Cr$_2$O$_3$, or SiO$_2$ [10], and suppression of TiO$_2$ as rutile growth [11]. Based on the thermodynamic stabilities of the these oxides, it can be derived that only alumina is a suitable oxide to

act as a protective scale in the case of γ-TiAl alloys, because both Cr_2O_3 and SiO_2 are less stable than TiO_2 at high operating temperatures.

A deposited coating, called thermal barrier coating (TBC), usually consists in several layers with different functionality, namely a top ceramic (TC) layer, a metallic bond coat (BC) and a thermally grown oxide (TGO) layer at the BC/TC interface formed during high temperature operation in air. Selection of the TBC's materials is ruled by the following parameters: low thermal conductivity, chemical inertness, high melting points and wear resistance, matching of the CTE with the substrate [1, 12]. The most known BC of MCrAlY (where M stands for Ni and Co) ensures oxidation protection and adhesion of TBC to the support [1] while the ceramic outer layer or the thermal barrier prevents overheating of the support due to its very low thermal transfer coefficients. In fact, TC reduces temperature of the TBC surface by 100-300°C range [13]. Moreover, the ceramic layers deposited by air plasma spraying (APS) as well as by high-velocity oxygen fuel spraying (HVOF) are porous and do not block the diffusion of oxygen to the support [14], a real diffusion barrier against oxygen is represented by the TGO layer grown between the bond coating and thermal barrier [15,16]. Given the fact that thermodynamically studies pointed out that α-Al_2O_3 is the most stable alumina polymorph [17] and a TGO of α-Al_2O_3 is difficult to obtain on titanium aluminides operating bellow 1100° C, in air [18], recently some researchers have been investigated possibility to deposit a sandwich layer of Al_2O_3 as a diffusion barrier included in a TBC system [8,19]. Also, top ceramic coats of Al_2O_3 and Al_2TiO_5/Al_2O_3 were applied to diminish oxygen diffusion inwards the γ-TiAl alloys [20].

Since α₂-Ti_3Al alloy does not develop a continuous layer of protective α-Al_2O_3 during oxidation, the purpose of our work was to deposit a Al_2O_3 layer by APS onto a NiCrAlY / Ti_3Al system and to study its behavior both as a diffusion barrier against oxygen and thermal barrier, during long isothermal oxidation at 850°C for 500 h. Results of this study will complete our previous reported data [21] on the same system exposed to cyclic oxidized conditions.

2. Materials and methods

The cast α₂-titanium aluminide with a chemical composition of Ti-19Al-10Nb-3V (at. %) and shaped into 20x20x2 mm specimens served as support material. Surface of the specimens were polished with emery paper, micro powder alumina and further ultrasonically cleaned in distilled water. Two types of coatings were successively deposited on the specimen surfaces by APS technique, a metallic coat of NiCrAlY (Amdry 9621) with a bonding role (BC) and a top ceramic coat consisting in α-Al_2O_3 (Metco 105NS), respectively. The main characteristics of the powders (Sulzer Metco) used to obtain these two coatings were presented in Table 1.

Table 1. The main characteristics of powders used in experiments

Powder	Ni (wt %)	Cr (wt %)	Al (wt %)	Y (wt %)	Grain size μm
NiCrAlY (Amdry 9621)	base	22	10	1	-90 ÷+45
α-Al_2O_3 (Metco 105 NS)	-	-	98.0	-	-45 ÷ +15

Both coatings were deposited by an Ar–H_2 plasma jet generated by means of a METCO 7 M gun operating at plasma arc power of 34 - 35 kW. The specific deposition parameters for the APS coating are illustrated in Table 2.

Table 2. Selected parameters for APS sprayed coatings

Parameters	Amdry 9621	Metco 105NS
Voltage (V)	68	70
Current (A)	500	500
Ar (L/min.)	45	40
H_2 (L/min.)	12	13
Powders feed rate (g/min.)	38	40
Spraying distance (mm)	120	120
Nozzle diameter (mm)	2	1.8

Thermal oxidation tests of all specimens were conducted in a Vulcan 3-130 Ney furnace at 850°C for 500 h, in air. The mass gain of each isothermal oxidized specimen was measured by using an analytical balance (accuracy ±0.1mg). Three identical specimens of each system were analyzed in order to confirm reproducibility.

The coatings characterization was carried out by microscopic and spectroscopic methods, as follows: Scanning Electron Microscopy (SEM), Raman Spectroscopy and X-ray diffraction.
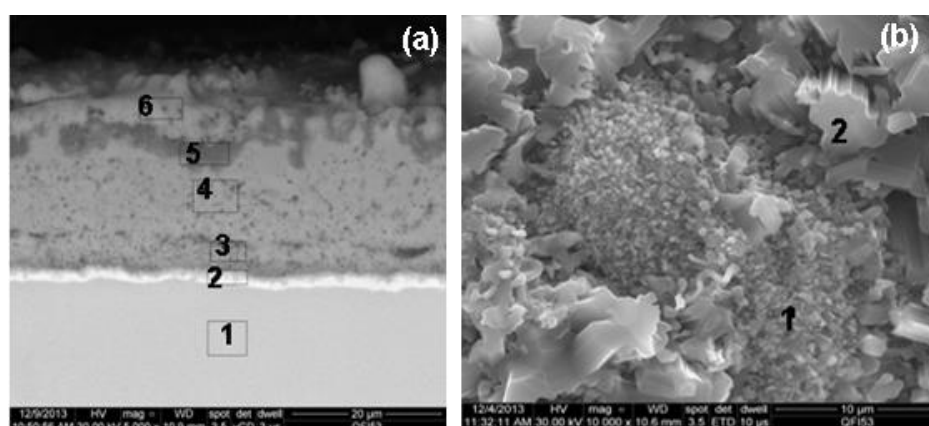
For morphological characterization a microscope FEI Inspect F50 high-resolution field emission equipped with energy dispersive spectroscopy (EDS) was used, while compositional and structural analysis were carried out by means of a micro-Raman spectrometer (LabRam HR800 from Jobin-Yvon–Horiba) equipped with a 514 nm laser and a Rigaku Ultima IV diffractometer with CuKα radiation, operating at 40kV and 30mA and equipped with a thin film attachment for grazing incidence X-ray measurements at an incidence angle ω=0.5°.

3. Results and discussions

3.1 α₂-Ti₃Al base alloy

The bare base alloy of α_2-Ti_3Al was strongly oxidized after 500 h exposure at 850°C. Thus, its surface is covered by a mixture of aluminum and titanium oxides with different morphologies as noticeable in Figure 1 and Table 3.

According to the transversal section in Figure 1a, thickness of the oxide formed coating is considerable reaching about 50-60µm. The layered structure of the grown oxide layer is in agreement with the one reported by Leyens [1] consisting in two main morphologies, here labeled 1 and 2, for small grain of rich aluminum oxides and blocks of columnar titanium rich oxides, respectively. However, due to discontinuous alumina layer and unprotective titanium dioxide formed on bare α_2-Ti_3Al alloy is prone to spallation [1].

Figure1. Cross-section (a) and surface (b) SEM images of α_2-Ti_3Al
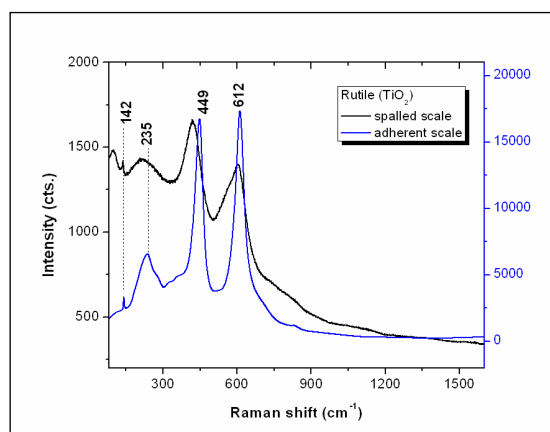after 500 h of thermal oxidation at 850 °C

This fact is also evidenced by EDX and Raman analysis of the specimen surface (Table 2 and Figure 2). As expected for high temperature exposure, the rutile polymorph [22] of TiO_2 is noticeable

in Figure 2. Lack of alumina evidence in the Raman spectra [23] collected from spalled and adherent scale is due to the fact that TiO_2 is a strong Raman scatterer [24] that masks other spectral contributions regardless its concentration. Shifted and broader bands for the spalled scale might be caused by the smaller crystal size and/or less crystalline grown TiO_2.

Table 3. Chemical compositions (analyzed by EDXS) of the zones in α_2-Ti_3Al after 500 h of thermal oxidation at 850 °C (wt. %)

Analy zed zone	O K	Al K	Nb L	Ti K	V K
1-fig.1a	4	19	10	64	3
2-fig.1a	7	16	20	41	6
3-fig.1a	26	2	13	51	8
4-fig.1a	26	2	9	55	8
5-fig.1a	35	39	2	21	3
6-fig.1a	47	28	2	20	3
Global surface	38	18	5	34	5
1-fig.1b	43	22	5	26	4
2- fig.1b	38	5	0	50	7

To improve long term oxidation resistance of the rich titanium alloys as α_2-Ti_3Al, deposition of protective layers is required.

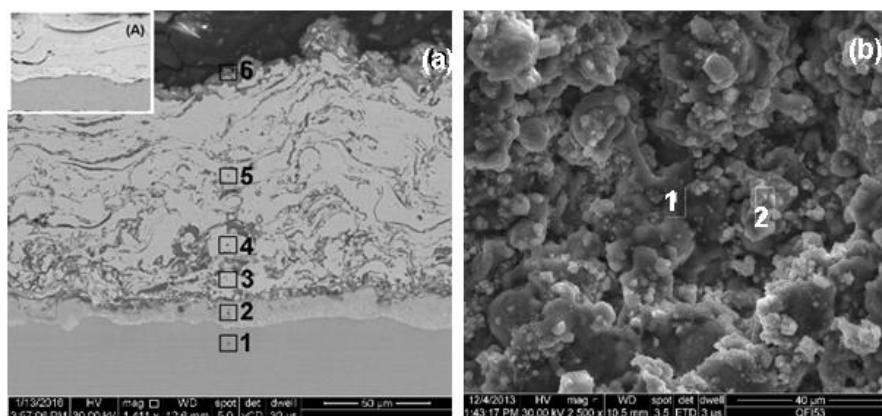**Figure 2**. Raman spectra of the oxide scale formed by α_2-Ti_3Al specimen

3.2 α_2-Ti_3Al coated with NiCrAlY

One of the protocols to improve oxidation resistance of the α_2-Ti_3Al alloy above 800 °C is to apply a protective layer of NiCrAlY as bond coat (BC) and subsequently to anchor a thermal ceramic (TC) coat [1].

The cross-section analysis of NiCrAlY / Ti_3Al specimen obtained in this work by APS is illustrated in Figure 3a. Adhesion between BC and substrate is relatively good since no discontinuities were found at the NiCrAlY-Ti_3Al interface. Moreover, several oxide stringers (dark grey streaks) in the inset A of the figure 3a suggest that weak particle oxidation occurred during deposition process. A plausible explanation for these defects in the APS coatings consists in shrinkage of the molten droplets as soon as they splat and rapidly solidify onto substrate [16]. Given the fact that porosity can affect negatively the oxidation resistance of the bond coats [25, 26], an estimated average porosity of 7.5%, obtained by SEM image analysis, for the NiCrAlY coat in this work points out its relatively dense state. Typically, porosity of the bond coat alloys deposited by plasma spraying methods can exceed 10%.

Figure 3. SEM images of surface and cross-section of NiCrAlY / Ti$_3$Al specimens after thermal oxidation at 850 °C for 500 h

Although absent in as-obtained NiCrAlY-Ti$_3$Al system, by 500-hour isothermal exposure at 850 °C a significant interdiffusion affected zone of about 20 µm into substrate is formed (see whitish zone 2 in Figure 3a).

The EDXS data and elemental map in figure 4-d show nickel as the main diffusing element from coating to substrate; its concentration reaches about 47% (point 2 in fig. 3a), while Ti diffuses from substrate to coating (Ti map in Figure 4f). A small concentration of chromium (2%) in the interdiffusion substrate zone, suggests its limited involvement.
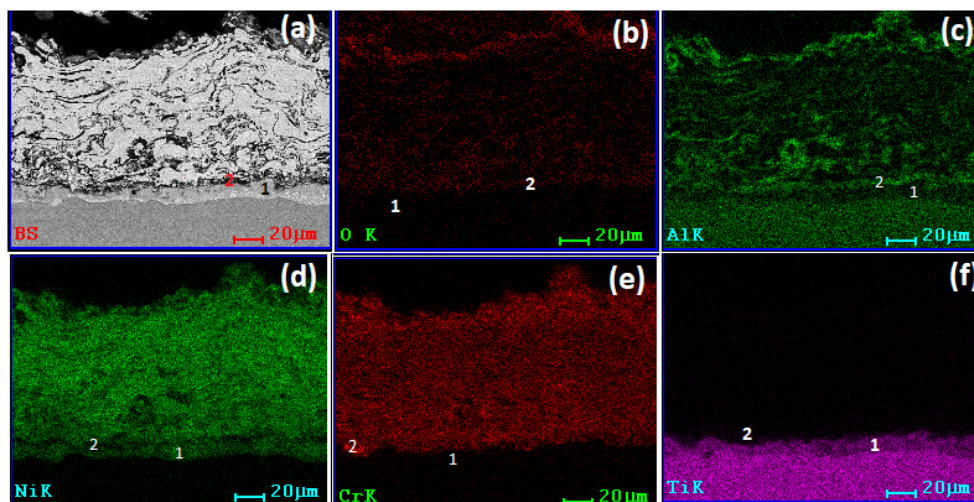
Table 4. Chemical compositions (analyzed by EDX) of the zones in
NiCrAlY / Ti$_3$Al after exposure at 850 °C for 500 h (wt. %)

Analyzed zone	O K	Al K	Y L	Cr K	Ni K	Ti K	Nb L	V K
1-fig.3a	-	19	-	-	-	68	10	3
2-fig.3a	-	13	-	2	48	29	6	2
3-fig.3a	4	7	2	27	56	2	2	-
4-fig.3a	2	9	3	16	70	-	-	-
5-fig.3a	2	9	3	18	68	-	-	-
6-fig.3a	23	27	2	12	36	-	-	-
Global surface	19	20	2	19	40	-	-	-
1-fig.3b	30	38	2	12	18	-	-	-
2- fig.3b	17	8	-	12	63	-	-	-

According to elemental distribution maps presented in Figure 4 it can be assumed that the inferior side of the thin layer formed between substrate and coating is bordered by small aluminum and chromium rich phase due to an inward diffusion of Ni as discussed above. Hence, by longtime oxidation (500 h at 850°C) of the NiCrAlY/ Ti$_3$Al specimens, a grey layer with a thickness of about 5µm at the coating/substrate interface was depicted in Figure 3a between zones 2 and 3. This layer is mainly composed of Cr$_2$O$_3$ and a small quantity of Al$_2$O$_3$ according to EDXS analysis (Table 4) and elemental distribution maps (zone 2 in Figures 4-a, b, c, e). Cr$_2$O$_3$ formation can be ascribed to selective internal oxidation. High affinity of oxygen for chromium and aluminum is the reason for obtaining beneficial Al and Cr oxides with higher stability.
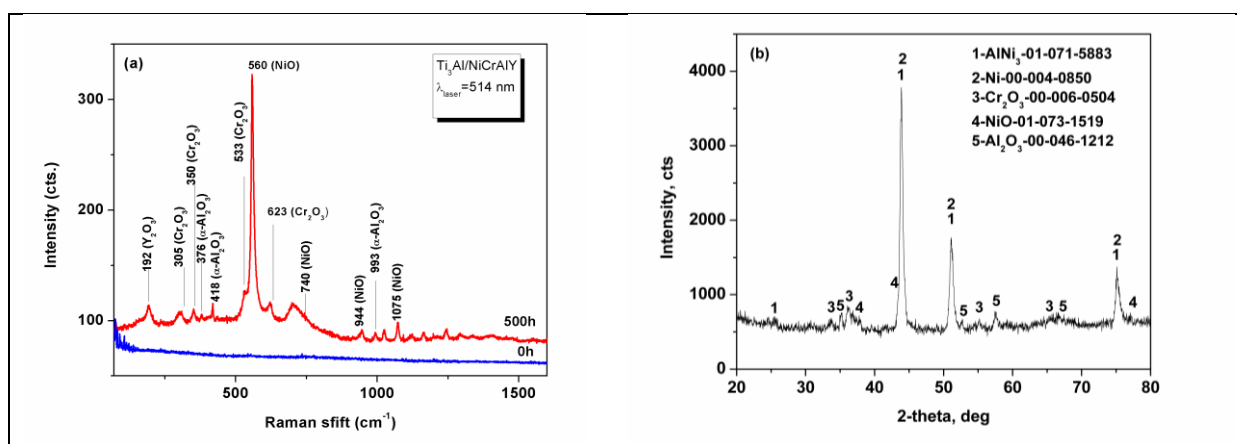
Furthermore, a very thin discontinuous outer layer (Figure 3a - point 6 and Figures 4-b, c, d, e) was grown on NiCrAlY coating by long isothermal oxidation. According to Figures 3b, 4-b, c and 4-d, e the outer oxide scale consists in alumina disrupted by nickel and chromium oxides.

Figure 4. Elemental distribution maps of cross-section of NiCrAlY / Ti_3Al specimen after exposure 500 h at 850 °C

Raman spectrum_500h in Figure 5a point out an intricate composition (Figure 5 and Table 4) of the TGO layer, namely: NiO (bands located at 560, 740 and 1075 cm^{-1} [27]), low amounts of Y_2O_3 (band at 192 cm^{-1} [28]) and Cr_2O_3 (305, 350, 533, 623 cm^{-1} bands [29]) scale and traces of α-Al_2O_3 (418 and 993 cm^{-1} bands [23]). As expected, no Y and Al oxides were depicted with Raman analysis on the NiCrAlY/Ti_3Al specimen prior oxidation test, namely the NiCrAlY / Ti_3Al_0h spectrum in Figure 5a. XRD analysis of isothermal oxidized NiCrAlY / Ti_3Al specimen oxidized revealed the presence of Cr_2O_3, Al_2O_3, NiO as well as Ni, $AlNi_3$ (Figure 5b). No diffraction lines corresponding to Y_2O_3 (as was confirmed by Raman spectroscopy) were observed probably due to their lower amount under XRD limit detection (< 5%). Large amount of NiO, traces of α-Al_2O_3 and no TiO_2 were formed during long isothermal oxidation tests at 850° C carried out in this work (Raman spectrum_500h in Figure 5a) in comparison with the NiCrAlY / Ti_3Al specimens cyclic oxidized (10 times x 10 h) at 850° C where transient aluminas were depicted [21].

Figure 5. (a) Raman spectra of the NiCrAlY / Ti_3Al specimen initial state (0h) and oxidized at 850 °C for 500 h, and (b), XRD pattern of the NiCrAlY / Ti_3Al specimen oxidized at 850°C for 500 h
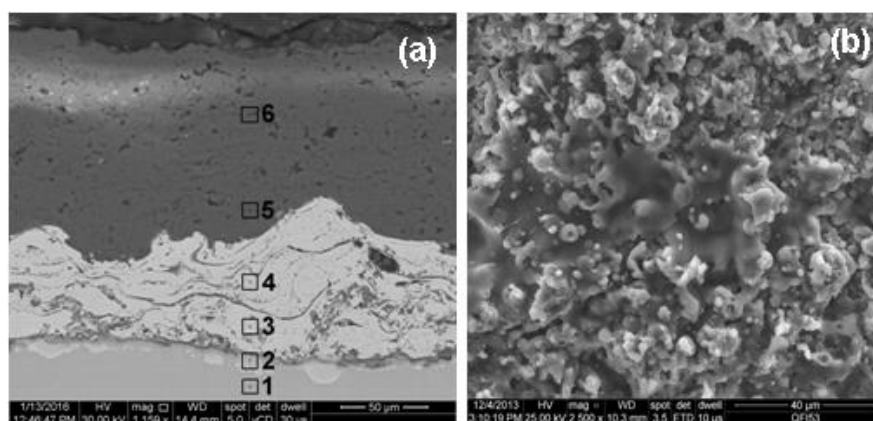
Conversely, TGO of the long isothermal treated specimens here are also similar with the preoxidized treated NiCrAlY / Ti_3Al specimens at 1100°C for 2h presented in our prior paper [21]. The latter specimens exposed to cyclic oxidation (10 times x 10 h) at 850°C had a TGO consisting in a

mixture of $NiCr_2O_4$ spinels and higher content of corundum (α-Al_2O_3). Hence, preoxidation treatment at high temperatures (>1000° C) enables formation of richer-α-Al_2O_3 TGO.

However, discontinuous α-Al_2O_3 and detrimental NiO present in the scale requires an additional diffusion barrier layer on the NiCrAlY / Ti_3Al specimen surface.

3.3 α_2-Ti_3Al coated with Al_2O_3 / NiCrAlY

α-Al_2O_3 was selected to cover the NiCrAlY / Ti_3Al system in order to protect against interdiffusion processes as well as inward oxygen diffusion. The new Al_2O_3 / NiCrAlY / Ti_3Al system was tested with respect of both diffusion and thermal barrier roles. Although alumina coat deposited by APS technique consists in metastable and amorphous aluminas [18], few strategies (various oxide additions [18], laser surface treatment and annealing above 1000 °C [30]) were used to convert metastable aluminas into α-Al_2O_3. Since annealing treatment of the APS deposited alumina coat causes formation of micro-cracks and volume reduction of the coat, no pre-oxidation treatment was applied to the Al_2O_3 / NiCrAlY / Ti_3Al system.

Figure 6. SEM images of surface and cross-section of
Al_2O_3 / NiCrAlY / Ti_3Al specimens after 500 hours of thermal oxidation at 850 °C
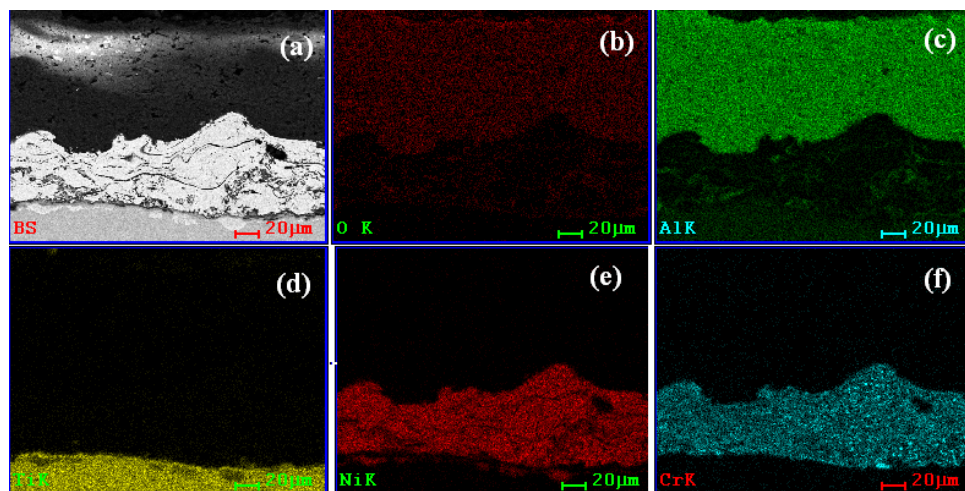
According to the SEM image in Figure 6a, diffusion processes between the α_2-Ti_3Al support and the NiCrAlY coating were diminished (Figure 6). This fact is supported by the elemental analysis in Table 5 and Ni map in Figure 7c.

Table 5. Chemical compositions (analyzed by EDX) of the zones in
Al_2O_3 / NiCrAlY / Ti_3Al after 500 h of thermal oxidation at 850 °C (wt. %)

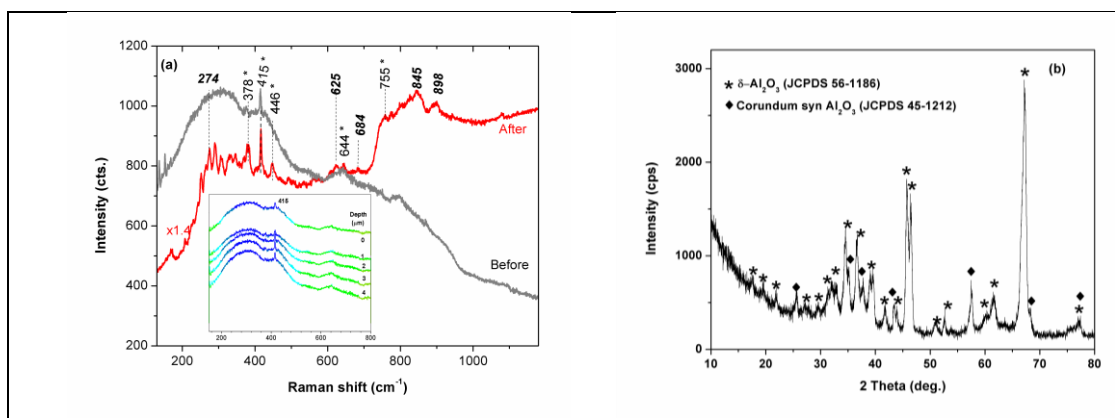| Analyzed zone	O K	Al K	Y L	Cr K	Ni K	Ti K	Nb L	V K
1-fig.7b	-	19	-	-	-	68	10	3
2- fig.7b	-	14	-	-	27	49	7	3
3-fig.7b	2	8	1	17	71	1	-	-
4-fig.7b	2	10	-	20	68	-	-	-
5-fig.7b	34	66	-	-	-	-	-	-
6-fig.7b	34	66	-	-	-	-	-	-
Global-surface	34	66	-	-	-	-	-	-

The nickel diffusion is two times smaller than the one recorded for the specimens coated with only NiCrAlY. It can be concluded that the top Al_2O_3 layer hindered the interdiffusion processes at the NiCrAlY-Ti_3Al interface.

EDX analysis (zones 3 and 4 in Figure 6a and Table 5) and elemental distribution maps in Figures 7 b-c-f point out traces of several oxides (especially Al and Cr), very likely formed either during deposition process or long isothermal oxidation at 850 °C. A plausible explanation consists in presence of less dense top coat of Al_2O_3 (Figure 6b) which allows oxygen diffusion towards the bond coat and hence internal oxidation (Figures 7 b-c-e-f).

Figure 7. Elemental distribution map of cross-section of Al_2O_3 / NiCrAlY / Ti_3Al specimen after 500 h of thermal oxidation at 850 °C

Presence of transient and/or amorphous aluminas along with traces of dense and protective α-Al_2O_3 are noticeable in Raman spectrum (Figure 8a) of the alumina top coat before exposure to isothermal oxidation. Intriguingly the amount of α-Al_2O_3 polymorph seems to increase as the depth increases (see depth profile Raman spectra in the inset of Figure 8a). Although isothermal oxidation test was conducted bellow 1000 °C, crystallization of δ - θ and α polymorphs of Al_2O_3 are inferred from the Raman spectrum_after [31] and XRD patterns in Figure 8.
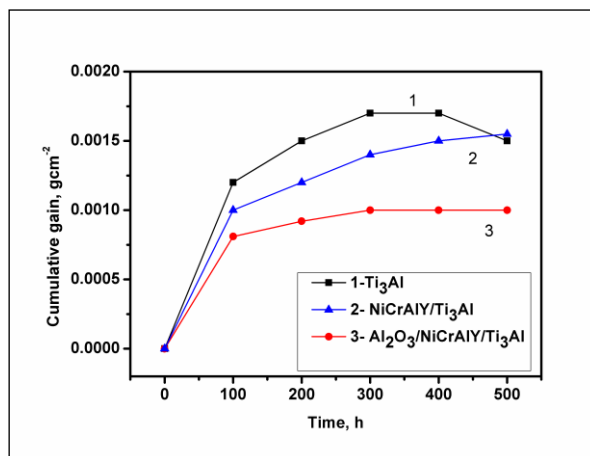

Figure 8. (a) Raman spectra (* stands for α-Al_2O_3 and inset represents the depth profile spectra before oxidation) and (b), XRD pattern of the Al_2O_3 / NiCrAlY / Ti_3Al specimen oxidized at 850 °C for 500 h

By heating above 800°C, gradual crystallization of α-Al_2O_3 is accompanied by densification and lowering of the alumina coat porosity and hence diminishing of the oxygen diffusion through the coating.

Figure 9 shows the mass gain for uncoated and coated specimens during isothermal oxidation at 850°C. Specimens coated with NiCrAlY and Al_2O_3 / NiCrAlY did not fail by spallation during the maximum exposure time, whereas the specimen uncoated exhibits the worst oxidation resistance. The mass gain rate of all specimens was rather steep at the beginning of isothermal oxidation test. Conversely, similar mass gain was recorded for the same specimen pre-annealed at 1100 °C and exposed to cyclic oxidation [21]. After 100 h of oxidation, the specimen coated with diffusion barrier (α-Al_2O_3) exhibits better oxidation resistance than the uncoated and NiCrAlY-coated specimens.

Figure 9. Plot of mass gain vs. time during the isothermal
oxidation at 850°C of Ti_3Al, NiCrAlY / Ti_3Al and Al_2O_3 / NiCrAlY / Ti_3Al

Decreasing mass gain rate of the alumina-covered specimens illustrated in Figure 9 could be explained by formation of denser and richer α-Al_2O_3 coat when exposed to high temperature for long time. Hence, we can assume that in time the outer alumina coating acts as an oxygen diffusion barrier and protects inner layers against oxidation. This assumption is supported by oxygen concentration measurements performed inside of the bond coating, at 20 µm under alumina coating after different oxidation times, e.g. 300 h- 11 wt %, (results not shown here); 500 hours-2 wt % (Table 5 zones 3 and 4).

Furthermore, a mass gain of about 0.8- 0.95 mg cm^{-2} for the Al_2O_3 / NiCrAlY / Ti_3Al specimens during 500 h of isothermal oxidation at 850°C is consistent with data reported for other thermal barrier coatings (0.8-1.4 mg cm^{-2} for YSZ / NiCrAl / TiAl) [32] and our previous results for Al_2O_3 / NiCrAlY / Ti_3Al during cyclic oxidation at 850 °C (0.97 mg cm^{-2})[21].

4. Conclusions
A new Al_2O_3 / NiCrAlY / Ti_3Al system obtained by APS technique was tested for isothermal oxidation resistance at 850°C for 500 h.

It can be concluded that the top coat of Al_2O_3 has substantially declined oxidation rate for isothermal oxidation of Al_2O_3 / NiCrAlY / Ti_3Al due to its dual role of oxygen and thermal barrier. However, without annealing treatment of α-Al_2O_3 formation, the Al_2O_3 / NiCrAlY / Ti_3Al system should be used in milder operating conditions, e.g. where cyclic oxidation resistance is not required.

References

1. LEYENS, C., PETERS, M., *Titanium and Titanium Alloys: Fundamentals and applications*, Wiley-VCH Verlag GmbH, Wenheim, ISBN: 3-527-30534-3, 2003, 201-230.

2. GHERGHESCU, I. A., SORIN CIUCA, S., JICMON, G. L., DUMITRESCU, R. E., BRANZEI, M., Thermal Cycling Influence on the Transformation Characteristics of a Ni50Ti48Nb2 Shape Memory Alloy, *Rev.Chim.,* **68** (5), 2017, 991-996. https://doi.org/10.37358/RC.17.5.5596

3. QU, S.; TANG, S.; FENG, A.; FENG, C.; SHEN, J.; CHEN, D. Microstructural evolution and high-temperature oxidation mechanisms of a titanium aluminide based alloy, *Acta Mater.,* **148** (4), 2018, 300-310. https://doi.org/10.1016/j.actamat.2018.02.013

4. OUYANG, P., MI, G., LI, P., HE, L., CAO, J., HUANG, X., Non-Isothermal Oxidation Behaviors and Mechanisms of Ti-Al Intermetallic Compounds, *Materials* **12** (13), 2019, 2114-2135. https://doi.org/10.3390/ma12132114

5. MARCU, M., BANU, A., ANGHEL, E.M., PARASCHIV, A., Corrosion Behavior of a Thermally Oxidized Orto-Titanium Aluminide in Synthetic Seawater, *Int. J. Electrochem. Sci.,* **10** (10), 2015, 8284-8297.

6. BANU, A., MARCU M., PETRESCU, S., IONESCU, N, PARASCHIV, A., Effect of niobium alloying level on the oxidation behavior of titanium aluminides at 850°C, *Int. J. Min. Met. Mater.,* **23** (12), 2016, 1452–1457. https://doi.org/10.1007/s12613-016-1369-y

7. KIM, S-W., HONG, J.K., NA, Y-S., YEOM, J-T., KIM S.E., Development of TiAl alloys with excellent mechanical properties and oxidation resistance, *Mater. Des.*, **54** (2), 2014, 814-819. https://doi.org/10.1016/j.matdes.2013.08.083

8. Li, H.Q., WANG, Q.M., JIANG, S.M., MA, J., GONG, J., SUN, C., Oxidation and interfacial fracture behavior of NiCrAlY/Al$_2$O$_3$ coatings on an orthorhombic –Ti$_2$AlNb alloy, *Corros. Sci.,* **53** (3), 2011, 1097-1106. https://doi.org/10.1016/j.corsci.2010.12.007

9. SHANABARGER MR., Comparative study of the initial oxidation behavior of a series of titanium–aluminum alloys, Appl. Surf. Sci., **134** (1), 1998, 179-186.

10. SINGHEISER, L., NIEWOLAK, L., FLESCH, U., SHEMET, V., QUADAKKERS, W.J., Fundamental considerations for the development of oxidation-resistant alloys and coatings based on γ-TiAl, *Metall. Mater. Trans. A,* **34** (10), 2003, 2247–2251. https://doi.org/10.1007/s11661-003-0288-5

11. VOJTĚCH, D., POPELA, T., KUBASEK, J., MAIXNER, J., NOVAK, P., Comparison of Nb- and Ta-effectiveness for improvement of the cyclic oxidation resistance of TiAl-based intermetallics, *Intermetallics*, **19** (4), 2011, 493-501. https://doi.org/10.1016/j.intermet.2010.11.025

12. MOSKAL, G., Thermal barrier coatings: characteristics of microstructure and properties, generation and directions of development of bond, *J. Achiev. Mater. Manuf. Eng.,* **37** (2), 2009, 323-331

13. LIU, Y.Z, HU, X.B., Segregation and microstructural evolution at interfaces of atmospheric plasma sprayed thermal barrier coatings during thermal cycling, *J. Alloy. Compds.*, **819**, 2020, article 153026 https://doi.org/10.1016/j.jallcom.2019.153026

14. BANU, A., MARCU, M., TRUSCA, O., PARASCHIV, A., ANGHEL, E.M., ATKINSON, I., Microstructural Characterization of NiCrFeSiBC Coating During Long-Term Isothermal Oxidation at 850 °C, *J. Therm. Spray Technol.,* **28** (6), 2019, 1275–1283. https://doi.org/10.1007/s11666-019-00881-1

15. LIU, Y.Z., HU, X.B., ZHENG, S.J., ZHU, Y.I., WEI, H., MA, X.I., Microstructural evolution of the interface between NiCrAlY coating and superalloy during isothermal oxidation, *Mater. Des.,* **80** (9) 2015, 63-69. https://doi.org/10.1016/j.matdes.2015.05.014

16. RICHER, P., YANDOUZI, M., BEAUVAIS, L., JODOIN B., Oxidation behaviour of CoNiCrAlY boand coats produced by plasma, HVOF and cold dynamic sprayed, *Surf. Coat. Technol.,* **204** (24), 2010, 3962-3974. https://doi.org/10.1016/j.surfcoat.2010.03.043

17. LEVIN, I., BRANDON, D., Metastable Alumina Polymorphs: Crystal Structures and Transition Sequences, *J. Am. Ceram. Soc.,* **81** (8), 1998, 1995-2012. https://doi.org/10.1111/j.1151-2916.1998.tb02581.x

18. ILAVSKY, J., BERNDT, C.C., HERMAN, H., CHRASKA, P., DUBSKY, J., Alumina-base plasma-sprayed materials-Part II: Phase transformations in aluminas, *J. Therm. Spray Technol.,* **6** (4), 1997, p. 439-444. https://doi.org/10.1007/s11666-997-0028-2

19. DING, Z.Y., WANG, Y.H., OUYANG, J.H., LIU, Z.G., WANG, Y.M., WANG, Y.J., Influence of Al_2O_3 addition in $NaAlO_2$ electrolyte on microstructure and high-temperature properties of plasma electrolytic oxidation ceramic coatings on Ti_2AlNb alloy, *Surf. Coat. Technol.,* **370** (7), 2019, p. 187-195. https://doi.org/10.1016/j.surfcoat.2019.04.075

20. Zhang, X.J., Li, Q., Zhao, S.Y., Gao, C.X., Wang, L., Zhang J., Improvement in the oxidation resistance of a γ-TiAl-based alloy by sol–gel derived Al_2O_3 film, *Appl. Surf. Sci.*, **255** (5), 2008, 1860-1864. https://doi.org/10.1016/j.apsusc.2008.06.041

21. ANGHEL, E.M., MARCU, M., BANU, A., ATKINSON, I., PARASCHIV, A., PETRESCU,S., Microstructure and oxidation resistance of a NiCrAlY/Al_2O_3-sprayed coating on Ti-19Al-10Nb-V alloy, *Ceram. Int.*, **42** (10), 2016, 12148–12155. https://doi.org/10.1016/j.ceramint.2016.04.148

22. BALACHANDRAN, U., EROR, N.G., Raman spectra of titanium dioxide, *J. Solid State Chem.,* **42** (3), 1982, 276-282. https://doi.org/10.1016/0022-4596(82)90006-8

23. PORTO, S.P.S., KHRISHNAN, R.S., Raman effect of corundum, *J. Chem. Phys.,* **47** (3), 1967, 1009-1012. https://doi.org/10.1063/1.1711980

24. BUIXADERAS, E., ANGHEL, E.M., PETRESCU, S., OSICEANU, P., Structural investigation in the TiB_2–($Na_2OB_2O_3$ Al_2O_3) system, J. Solid State Chem., **183** (9), 2010, 2227-2235 https://doi.org/10.1016/j.jssc.2010.07.023

25. ODHIAMBO, J.G., LI W.G., ZHAO, Y.T., LI, C.L., Porosity and Its Significance in Plasma-Sprayed Coatings, *Coatings*, **9** (7), 2019, 460-479. https://doi.org/10.3390/coatings9070460

26. PLANQUES, P., VIDAL, V., LOURS, P., PROTON, V., CRABOS, F., HUEZ, J., VIGUIER B., Mechanical and Thermo-physical Properties of Plasma-Sprayed Thermal Barrier Coatings: A Literature Survey*, Oxid. Met.,* **88** (1-2), 2017, 133-143. https://doi.org/10.1007/s11085-016-9693-1

27. MARCIUS, M., RISTIC, M., IVANDA, M., MUSIC, S., Formation and microstructure of nickel oxide films, *J. Alloys Compd.,* **541**, 2012, 238-243. https://doi.org/10.1016/j.jallcom.2012.07.021

28. BARSHILIA, H.C., CHAUDHARY, A., KUMAR P., MANIKANDANATH, N.T., Wettability of Y_2O_3: A Relative Analysis of Thermally Oxidized, Reactively Sputtered and Template Assisted Nanostructured Coatings, *Nanomaterials,* **2** (1), 2012, 65-78. https://doi.org/10.3390/nano2010065

29. MOUGIN, J., ROSMAN, N., LUCAZEAU, G., GALERIE, A., In situ Raman monitoring of chromium oxide scale growth for stress determination, *J. Raman Spectrosc.,* **32** (9), 2001, 739-744. https://doi.org/10.1002/jrs.734

30. WANG, D, TIAN, Z., SHEN, L., LIU, Z., HUANG, Y., Influences of laser remelting on microstructure of nanostructured Al_2O_3–13 wt.% TiO_2 coatings fabricated by plasma spraying, *Appl. Surf. Sci.,* **255** (8), 2009, 4606-4610. https://doi.org/10.1016/j.apsusc.2008.11.082

31. DEO, G., HARDCASTLE, F. D., RICHARDS, M., HIRT, A. M., WACHS, I. E., (1990). Chapter 29: Raman Spectroscopy of Vanadium Oxide Supported on Alumina, in Novel Materials in Heterogeneous Catalysis; Baker, R., et al.; ACS Symposium Series; American Chemical Society: Washington, DC, 1990, 317-328. DOI: 10.1021/bk-1990-0437.ch029

32. BRAUN, R., FROHLICH, M., EBACH-STAHL, A., LEYENS, C., Investigation on the oxidation behaviour of gamma titanium aluminides coated with thermal barrier coatings, *Mater. Corros.,* **59** (7), 2008, 539-546. https://doi.org/10.1002/maco.200804136